Applied Catalysis B: Environmental 180 (2016) 424–433

Contents lists available at ScienceDirect

Applied Catalysis B: Environmental

journal homepage: www.elsevier.com/locate/apcatb

Direct methane oxidation on $La_{1-x}Sr_xCr_{1-y}Fe_yO_{3-\delta}$ perovskite-type oxides as potential anode for intermediate temperature solid oxide fuel cells

C. Aliotta [a,*], L.F. Liotta [b], F. Deganello [b], V. La Parola [b], A. Martorana [a]

[a] Dipartimento di Fisica e Chimica, edificio 17, viale delle Scienze, I-90128 Palermo, Italy
[b] Istituto per lo Studio dei Materiali Nanostrutturati, Consiglio Nazionale delle Ricerche, via U. La Malfa, 153, I-90146 Palermo, Italy

ARTICLE INFO

Article history:
Received 1 March 2015
Received in revised form 3 June 2015
Accepted 11 June 2015
Available online 17 June 2015

Keywords:
Doped-$LaCrO_3$
IT-SOFC
Direct methane oxidation
H_2S

ABSTRACT

$La_{1-x}Sr_xCr_{1-y}Fe_yO_{3-\delta}$ ($x = 0, 0.1, 0.15, 0.2$; $y = 0, 0.3, 0.5$) perovskite-type oxide powders were synthesized by solution combustion synthesis and characterized by X-ray diffraction, X-ray photoelectron spectroscopy and H_2-temperature programmed reduction. Selected compositions were studied by CH_4-temperature programmed reduction in the absence and in the presence of H_2S. Temperature programmed oxidation and structural characterizations were performed in order to discriminate the nature of residual deposits on the catalyst surface. The study about reduction in different methane-based mixture revealed that total and partial methane oxidation occurred in the range ~450–1000 °C independently of methane concentration. The H_2S influence on methane oxidation was evaluated and experiments in CH_4/H_2S gas mixture indicated that $La_{0.9}Sr_{0.1}Cr_{0.7}Fe_{0.3}O_{3-\delta}$ oxidized CH_4 to CO_2 and CO, as well as H_2S to SO_2. $La_{0.9}Sr_{0.1}Cr_{0.7}Fe_{0.3}O_{3-\delta}$ was therefore identified a potential anode material for intermediate temperature solid oxide fuel cells directly fed with CH_4 in the presence of H_2S.

1. Introduction

Solid oxide fuel cells working at intermediate temperature (IT-SOFCs) represent a valid alternative technology for providing clean energy, due to their ability to directly oxidize methane obtained by industrial and municipal wastes or energy crops [1]. Renewable methane-based fuels, like biogas and natural gas, might be therefore employed for the direct internal reforming of methane at the intermediate temperature range, i.e. ~500–850 °C. These fuels, however, contain traces of H_2S, a sulphur poison font, able to negatively affect the overall performance of the fuel cell. As a matter of fact, both sulphur and carbon deposits over the surface of anode material are considered the major limiting factors for the development of IT-SOFC fuelled with biogas or natural gas [2–4].

In principle, the desirable electrochemical anode reaction under IT-SOFC regime ought to be the total oxidation of methane to carbon dioxide, Eq. (1), although the formation of CO through the partial oxidation reaction, Eq. (2), can simultaneously take place [5]:

$$CH_4 + 4O^{2-} \rightarrow CO_2 + 2H_2O + 8e^- \quad (1)$$

$$CH_4 + O^{2-} \rightarrow CO + 2H_2 + 2e^- \quad (2)$$

It is well known that other parallel reactions involving the products of Eqs. (1) and (2) might occur upon the surface of the anode catalyst, for instance methane steam and dry reforming reactions leading to syngas [5]. However, the main risk for the lifetime of the anode catalyst is represented by the cracking of methane, Eq. (3), with the deposition of carbonaceous deposits on the active sites of anode material [6,7]:

$$CH_4 \leftrightarrow C + 2H_2 \quad (3)$$

Water production during the total methane oxidation may reduce carbon coke formation occurring at high temperature [2,5]. On the whole, carbon deposition may be avoided, or at least limited, by the continuous incoming to the anode of oxide ions transferred from the cathode. As a further drawback of renewable fuels, the presence of H_2S in the feed may give rise to sulphur deposition that deactivates the anode. This issue requires that the anode catalyst should be able to oxidize H_2S to easily removable species, avoiding S_x formation under IT-SOFC conditions [3].

Several studies concerning the resistance of the anode material towards carbon deposition have been reported in literature, and more recently even towards H_2S poisoning. Currently, the most common anode material for IT-SOFC is Ni-based cermet, namely nickel dispersed over the same material of the electrolyte, that provides catalytic activity towards fuel oxidation and mixed ionic-electronic conduction [1]. However, the nickel component easily

* Corresponding author.
E-mail address: chiara.aliotta@unipa.it (C. Aliotta).

http://dx.doi.org/10.1016/j.apcatb.2015.06.012
0926-3373/

Table 1
Label, space group, weight phase fraction (wt%) with relative volume (V) and lattice parameters (a, b, c) of LSCrFs. $LaCrO_3$ and LSCrF10 contain traces of La_2CrO_6 and $SrCrO_4$, respectively. LSCrF2050 contain 10 wt% of $SrCrO_4$. Uncertainty is on the last digit for volumes and cell parameters; uncertainty for wt.% is ≤3%.

Samples	Label	Space group	wt.%	V(Å^3)	a (Å)	b (Å)	c (Å)
$LaCrO_3$	$LaCrO_3$	Pbmn	98	234.80	5.5175	5.4813	7.7621
$La_{0.9}Sr_{0.1}CrO_{3-\delta}$	LSCrF10	Pbmn	83	234.24	5.5156	5.47633	7.7550
		R-3c	16	350.44	5.5085	5.5085	13.3356
$La_{0.9}Sr_{0.1}Cr_{0.7}Fe_{0.3}O_{3-\delta}$	LSCrF1030	Pbmn	85	235.78	5.5238	5.4923	7.7718
		R-3c	15	353.95	5.5198	5.5198	13.4141
$La_{0.9}Sr_{0.1}Cr_{0.5}Fe_{0.5}O_{3-\delta}$	LSCrF1050	Pbmn	100	237.92	5.5369	5.5111	7.7968
$La_{0.85}Sr_{0.15}Cr_{0.5}Fe_{0.5}O_{3-\delta}$	LSCrF1550	Pbmn	100	237.52	5.5370	5.5060	7.7909
$La_{0.8}Sr_{0.2}Cr_{0.5}Fe_{0.5}O_{3-\delta}$	LSCrF2050	Pbmn	51	238.18	5.5435	5.5145	7.7915
		R-3c	39	355.72	5.5276	5.5276	13.4434
LSCrF1030 treated in 0.3% CH_4		Pbmn	34	237.39	5.5427	5.4981	7.7900
		R-3c	66	354.82	5.5282	5.5282	13.4063
LSCrF1030 treated in CH_4/H_2S		Pbmn	52	236.36	5.5312	5.4983	7.7720
		R-3c	48	355.40	5.5263	5.5263	13.4377

undergoes coke poisoning during oxidation of methane-containing fuels, with deleterious consequence on material durability and cell performance. As a consequence, today the main challenge for IT-SOFC technology consists in developing active anode materials able to directly oxidize CH_4, as main component of renewable fuels, and simultaneously to avoid carbon and sulphur poisoning. Moreover, they must exhibit suitable mixed ionic-electronic conductivity under reducing atmosphere and high compatibility with the electrolyte material. In this light, perovskite-type oxides (ABO_3) represent a valid alternative to cermets, and in particular $LaBO_3$ (B = transition metal) compounds, as doped-$LaMnO_3$ or doped-$SrTiO_3$ have been widely investigated since they display high thermochemical stability at low pO_2 [2–4,8]. Among other candidates, it has been recently observed that Cr- and Fe-based perovskite oxides have suitable catalytic and electrocatalytic properties towards methane and H_2S oxidation [6,9,10–12]. Tao and Irvine [9] proposed $La_{0.75}Sr_{0.25}Cr_{0.5}Fe_{0.5}O_{3-\delta}$ as an alternative to the less active and more commonly used $La_{1-x}Sr_xCr_{0.5}Mn_{0.5}O_{3-\delta}$. Nevertheless, such compound exhibited satisfactory methane conversion at 900 °C only if CH_4 and O_2 were co-fed in at least equal molar ratio. Indeed, at that temperature the CO_2 formation is thermodynamically promoted by the O_2-rich conditions. More recently Danilovic et al. [10] proved that $La_{0.75}Sr_{0.25}Cr_{0.5}Fe_{0.5}O_{3-\delta}$, alone or intimately mixed with gadolinium-doped ceria, showed a more rewarding electrocatalytic activity towards methane oxidation compared to other B-site dopants like Mn, Co and Ti.

However, several literature papers dealt with new anode compositions for direct methane oxidation properly addressing the catalytic aspect, few of them treated this issue focusing on the reducibility features of the catalyst as key point for selecting an eligible anode material. Therefore, catalytic tests are necessary to evaluate both the effective temperature range and the resistance towards surface deactivation. Moreover, in the light of anode catalyst for IT- SOFC it is mandatory to examine the ability of the catalyst to release spontaneously lattice oxygen ions, O^{2-}, since this feature is essential under IT-SOFC regime.

The present work aims to evaluate Sr- and Fe-doped lanthanum chromites as potential anode materials for IT-SOFC directly fed with methane. In this respect, a series of differently doped $La_{1-x}Sr_xCr_{1-y}Fe_yO_{3-\delta}$ was synthesized and characterized for reducibility in methane-rich gas mixture even in the presence of H_2S. Special attention was devoted to the formation of carbon and sulphur deposits after reducibility tests.

2. Experimental

$La_{1-x}Sr_xCr_{1-y}Fe_yO_{3-\delta}$ (x = 0, 0.1, 0.15, 0.2; y = 0, 0.3, 0.5) powders were prepared by solution combustion synthesis using $La(NO_3)_3{\cdot}6H_2O$ (99,99% Sigma–Aldrich), $Sr(NO_3)_2$ anhydrous (99,99% Sigma–Aldrich), $Cr(NO_3)_3{\cdot}9H_2O$ (99,99% Sigma–Aldrich) and $Fe(NO_3)_3{\cdot}9H_2O$ (99,99% Sigma–Aldrich) as metal precursors and citric acid ($C_6H_8O_7$ anhydrous, ≥99,5% Sigma–Aldrich) as combustion fuel. Ammonia (28 vol.% NH_3 in H_2O, ≥99,99% Sigma–Aldrich) was also added as pH regulator (pH ∼ 6) in order to dissociate the carboxylic functional groups of citric acid. According to propellants chemistry [13], the combustion reactions were carried out in stoichiometric condition (Φ = reducers-to-oxidizers molar ratio = 1) with a fuel-to-metal cations molar ratio set to 2. To achieve this purpose, ammonium nitrate (NH_4NO_3, ≥99,0% Sigma–Aldrich) was added to reaction mixture as oxidant additive. Metal nitrates, fuel and additives were dissolved in aqueous solution in a stainless steel beaker. The reducers-oxidizers mixture was stirred at 80 °C until a dark coloured gel was formed. By increasing the temperature, a black fluffy powder was formed in all doped compositions, whereas the as-burned $LaCrO_3$ powder was green. Then, the powders were fired in air at 1000 °C for 5 h. The doped compositions $La_{1-x}Sr_xCr_{1-y}Fe_yO_{3-\delta}$ were named LSCrFXY, where the digits X and Y represent the corresponding molar percentage concentration of the dopant (Sr and Fe, respectively) in the perovskite. Therefore, the $La_{0.9}Sr_{0.1}CrO_{3-\delta}$ was labelled as LSCrF10, while the $La_{0.9}Sr_{0.1}Cr_{0.7}Fe_{0.3}O_{3-\delta}$ was named as LSCrF1030. The complete list of the prepared samples and corresponding labels is reported in Table 1.

X-ray diffraction (XRD) measurements were collected with a Siemens D5005 X-ray powder diffractometer equipped with a curved graphite monochromator on the diffracted beam. The observed range 25–90° 2θ was scanned with a step size of 0.02° 2θ and an integration time of 3s per step. Rietveld refinement of the diffraction patterns was carried out by using the GSAS package [14] and the agreement factors ("R values") were generally acceptable. Chebyschev polynomials and Pearson VII functions were chosen for the background and for the peak profile fitting, respectively. In the structure refinement lattice constants, atomic coordinates, scale factors and full width at half maximum (FWHM) parameters were considered as variables.

The X-ray photoelectron spectroscopy analyses were performed with a VGMicrotech ESCA 3000Multilab, equipped with a dual Mg/Al anode. The spectra were excited by the unmonochromatized Al Kα source (1486.6 eV) run at 14 kV and 15 mA. The analyser operated in the constant analyser energy (CAE) mode. For the individual peak energy regions, a pass energy of 20 eV set across the hemispheres was used. Survey spectra were measured at 50 eV pass energy. The sample powders were analyzed as powder, mounted on a double-sided adhesive tape. The pressure in the analysis chamber was in the range of 10^{-8} Torr during data collection. La was chosen as a reference here due to its good stability in $LaCrO_3$ structure, the constant charging of the samples was then removed by referencing all the energies to the La $3d_{5/2}$ peak set to 833.7 eV [15]. The

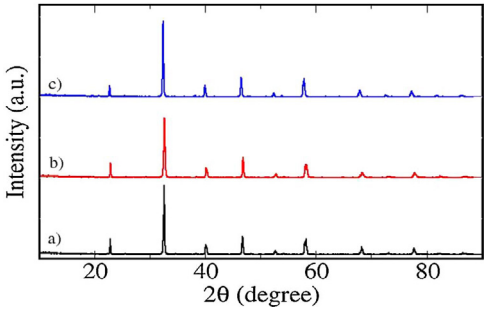

Fig. 1. XRD patterns of $LaCrO_3$ (a), LSCrF10 (b) and LSCrF1030 (c) obtained after firing at 1000 °C.

invariance of the peak shapes and widths at the beginning and at the end of the analyses ensured absence of differential charging. Analyses of the peaks were performed with the software provided by VG, based on non-linear least squares fitting program using a weighted sum of Lorentzian and Gaussian component curves after background subtraction according to Shirley and Sherwood [16,17]. Atomic concentrations were calculated from peak intensity using the sensitivity factors provided with the software. The binding energy values are quoted with a precision of ±0.15 eV and the atomic percentage with a precision of ±10%.

Reduction properties of the perovskite oxides were studied by temperature programmed reduction (TPR) measurements in H_2/Ar (5%, 30 ml/min) in the range between room temperature and 1000 °C (heating rate 10 °C/min). Experiments were carried out with a Micromeritics Autochem 2950 instrument equipped with a thermal conductivity detector (TCD) for the evaluation of hydrogen consumption through the use of proper calibration curves. All powders (~0.1 g) were pre-treated in O_2/He (5%, 50 ml/min) at 700 °C for 60 min and then cooled down under pure He.

CH_4-TPR tests in the presence of CH_4/He (0.3%, 50 ml/min), CH_4/He (3 vol.%, 50 ml/min) or CH_4/H_2S/He (3 vol.%/150 ppm, 50 ml/min) were performed in the range between room temperature and 1000 °C (heating rate 10 °C/min). The same instrument as for H_2-TPR, equipped with a mass quadrupole spectrometer (QMS Thermostar^{TM}, Balzers) was used in order to follow the evolution of all the species: CH_4, CO, CO_2, H_2, H_2O. Before CH_4-TPR tests, samples (~0.1 g) were pre-treated as above described for H_2-TPR. The concentration (vol.%) of CH_4, CO and CO_2 species during the reaction was measured by on line IR analyser (ABB Uras 14). After CH_4-TPR experiments performed in CH_4(3 vol.%)/He or in CH_4(3 vol.%)/H_2S(150 ppm)/He, the reduced catalysts were subjected to a successive temperature programmed oxidation (TPO) in order to investigate any CO_2 evolution arising from carbon coke deposit oxidation. In a typical TPO experiment, the samples were pre-treated under He flux up to 250 °C in order to remove physisorbed and chemisorbed C-rich species, then oxygen were flowed (5% in He, 50 ml/min) by increasing linearly the temperature from room temperature to 1000 °C. The temperature was kept at 1000 °C until all species were oxidized, and then the samples were cooled down to room temperature.

3. Results

3.1. Structural characterization

The XRD patterns acquired at room temperature from $LaCrO_3$ and doped-$LaCrO_3$ powders fired at 1000 °C are shown in Fig. 1. Rietveld-refined lattice parameters, volume phase and weight fraction percentages are listed in Table 1. As reported in the Supporting information (Fig. 1.1), $LaCrO_3$ exhibits an orthorhombic perovskite phase with traces of La_2CrO_6, while, in agreement with literature, doping the A-site with 10 at.% Sr leads to the co-existence of orthorhombic and rhombohedral LSCrF10 perovskite phases with traces of $SrCrO_4$ (Table 1, Supporting information Fig. 1.2) [18–20]. After a further thermal treatment at 1100 °C for 5 h, the monoclinic phases, La_2CrO_6 and $SrCrO_4$, can not be detected anymore in the diffraction patterns. In this context, it is worth noticing that Rietveld refinement permits to appreciate the small percentage of rhombohedral phase, also in those cases in which the peak convolution is not so well resolved. Moreover, due to the limited possibility of XRD to discriminate between elements with similar atomic number, in all cases in which two perovskite structures were detected, the Rietveld analysis was carried out assuming the same nominal composition for both phases.

Doping the A-site with Sr(II), whose 12-coordinated ionic radius is larger than La(III) [21] should induce an expansion of the unit cell, while charge balance, achieved by oxygen release and/or by oxidation of Cr(III) to Cr(IV), produces volume contraction. As a matter of fact, in LSCrF10 orthorhombic perovskite phase exhibits a reduced cell volume compared to the parent $LaCrO_3$ compound, likely due to the overall competing effects of ion hindrance and oxygen vacancy formation. As what concerns Fe-doping, it is noteworthy that iron is able to stabilize a single orthorhombic phase for Sr contents smaller than 20 at.% (Table 1). For these samples, the orthorhombic cell volumes grow with the amount of iron. This result relies on the presence of Fe(III)/Fe(IV) species having larger ionic radii than Cr(III)/Cr(IV).

Although some of the powders still contained the monoclinic impurities after a thermal treatment at 1000 °C, this temperature was chosen as the best one for all the examined powders, since it allows to maximise the perovskite component and, at the same time, to avoid the excessive decrease of the surface area and porosity taking place at higher temperatures.

In order to evaluate the chemical stability of doped lanthanum chromite immediately after reducing treatments at high temperature, XRD patterns were acquired after TPR in 0.3%CH_4 and 3%CH_4/150 ppmH_2S, as reported in Table 1 for LSCrF1030. In both cases, the tendency towards a higher amount of rhombohedral phase in reducing atmosphere can be recognized as it has been already observed by Tao and Irvine [9].

3.2. XPS Analysis

Selected samples were studied by XPS in order to identify the surface composition as a function of dopants content. Fig. 2 shows the Cr 2p peaks for the four selected different compositions. All oxides show at least three peaks for both $2p_{3/2}$ and $2p_{1/2}$ components. According to the literature, the peaks may be attributed to Cr(III) (ca. 575 eV), Cr(IV) (ca. 577 eV) and Cr(VI) (ca. 579 eV) [15]. LSCrF10 shows an increment of the Cr(VI) oxidized species with respect to the undoped $LaCrO_3$ (Table 2). The increase of Cr(VI) with the insertion of Sr in the structure was previously reported [22]. For the other Sr and Fe doped perovskite oxides, LSCrF1030 and LSCrF1050, the relative percentage of Cr(VI) detected on the surface is comparable to that of $LaCrO_3$ (Table 2). This is due to a counterbalancing effect of the iron insertion which, according to Bu et al. [11], would decrease the relative percentage of Cr(VI) with respect to Cr(III). As expected after exposure to reducing atmosphere, the Cr(VI) contribution disappears treating the samples in CH_4 (data not shown) and CH4/H_2S gas mixture (Table 2, Supporting information Fig. 2.1). Moreover, as evidenced by Table 2 the treatment under reaction mixture does not cause segregation or modification of the surface composition.

The Sr 3d region shows at least two doublets of the $Sr3d_{5/2}$–$Sr3d_{3/2}$ couple, even though no different species are expected in the Sr environment. Fig. 3 shows the Sr 3d spectra of the Sr doped samples and the fitting is shown for LSCrF1050 sam-

Table 2
XPS data of $LaCrO_3$ and selected LSCrFs in terms of Cr $2p_{3/2}$ and Sr $3d_{5/2}$ binding energies (in parenthesis the relative percentage of the different component are given) and B/A, Cr/A, Fe/A and Fe/Cr atomic ratios (in parenthesis the stoichiometric values are given). A and B refer to La or (La + Sr) and Cr or (Cr + Fe) atoms of the ABO_3 perovskite.

Sample	Cr $2p_{3/2}$	Sr $3d_{5/2}$	B/A	Cr/A	Fe/A	Fe/Cr
$LaCrO_3$	Cr(III) – 575.1 (48%), Cr(IV) – 576.4 (33%) Cr(VI) – 578.7 (19%)		0.8 (1)	0.8 (1)		
LSCrF10	Cr(III) – 575.4 (43%) Cr(IV) – 576.8 (24%) Cr(VI) – 579.4(33%)	132.6 (49%) 134.6 (51%)	0.7 (1)	0.7 (1)		
LSCrF1030	Cr(III) – 574.9 (49%) Cr(IV) – 576.4 (33%) Cr(VI) – 578.9 (18%)	132.5 (49%) 134.3 (51%)	0.6 (1)	0.4 (0.7)	0.1 (0.3)	0.24 (0.43)
LSCrF1050	Cr(III) – 575.5 (51%) Cr(IV) – 577.0 (30%) Cr(VI) – 579.5 (19%)	131.9 (49%) 134.0(51%)	0.6 (1)	0.4 (0.5)	0.2 (0.5)	0.55 (1)
Sample treated in CH_4/H_2S			B/A	S/(La + Cr)	Fe/A	Fe/Cr
$LaCrO_3$	Cr(III) – 575.6 (68%) Cr(IV) – 577.0 (32%)		0.8(1)	0.15		
LSCrF1030	Cr(III) – 575.7 (78%) Cr(IV) – 577.0 (22%)		0.4 (1)	0.28	0.1	0.2

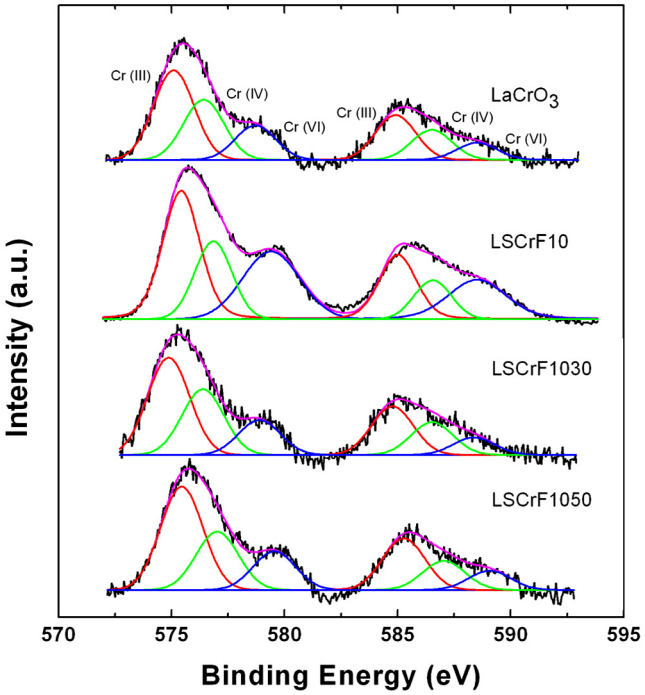

Fig. 2. High resolution Cr 3d region. Experimental signals (black lines), fitted model (magenta lines), Cr(III) contribution (red lines), Cr(IV) contribution (green lines) and Cr(VI) contribution (blue lines). (For interpretation of the references to color in this figure legend, the reader is referred to the web version of this article.)

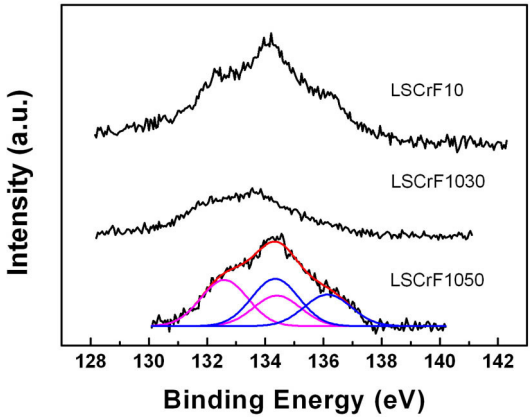

Fig. 3. High resolution XPS Sr 3d region. Experimental signals (black lines), fitted model (red line), Sr doublet (magenta line) and high energy Sr doublet (blue lines). (For interpretation of the references to color in this figure legend, the reader is referred to the web version of this article.)

ple, as an example. The presence of two different doublet signals of strontium is typical of the perovskite structure and the correct attribution of this pattern for the Sr region is not clear. According to Liu et al. [23] the higher binding energy component is attributed to Sr coordinated to 12 oxygen ions in the perovskites lattice, while the low energy component could be attributed to Sr surrounded by oxygen vacancies. Another hypothesis attributed the lower binding energy to the bulk component and the higher component to surface segregated strontium [24,25].

As what concerns the effect of Fe-doping, no difference is observed by increasing iron content. Iron peaks are typical of Fe(III) as indicated by the lack of the shake up satellite. This behavior is maintained even after CH_4/H_2S TPR tests (see Supporting information, Figs. 2.2–2.3).

Table 2 reports the binding energy of Cr $2p_{3/2}$ and Sr $3d_{5/2}$ along with the surface atomic concentration found by XPS, indicated as B/A ratio, Cr/A and Fe/A ratios, where A and B refer to La or (La + Sr) and Cr or (Cr + Fe) atoms of the ABO_3 perovskite. Looking at the B/A atomic ratios, in all cases an inward segregation of B site cations is observed. This trend is confirmed also by the Cr/A and Fe/A atomic ratios. Moreover, a Fe/Cr atomic ratio which is always half of the expected stoichiometric value substantiates a higher segregation of Cr with respect to Fe.

3.3. Reducibility

In order to evaluate the relative reducibility of each selected sample, H_2-TPR measurements were carried out up to 1000 °C. Fig. 4a shows TPR profiles for $LaCrO_3$ and for selected doped $LaCrO_3$ oxides. H_2 consumption values per gram of catalyst are summarized in Table 3. $LaCrO_3$ reduction curve is dominated by a broad peak at ~410 °C, which was ascribed to the partial reduction of Cr species having high valence, like IV or VI. [22,26–28]. In the same temperature range, the doped samples exhibit a broader and overlapped peak, which corresponds to a more significant H_2 con-

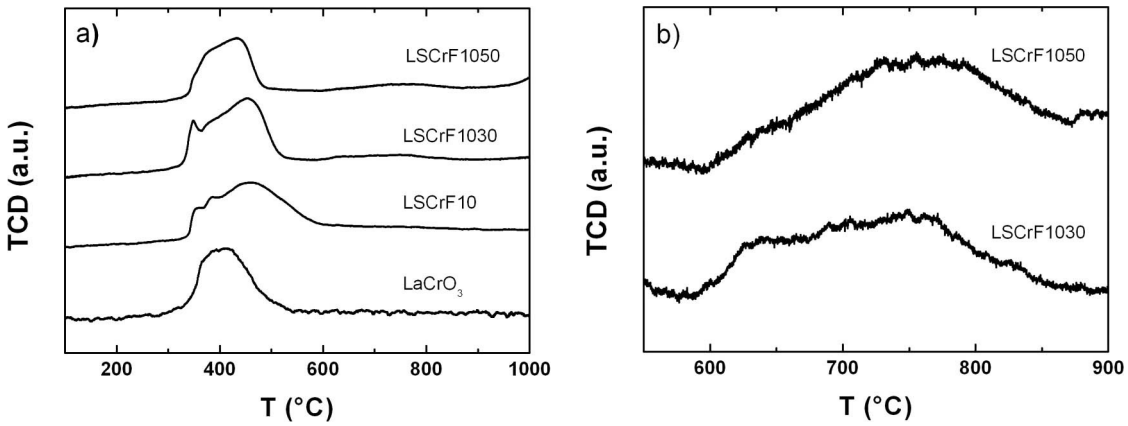

Fig. 4. H_2-TPR profiles of $LaCrO_3$, LSCrF10, LSCrF1030 and LSCrF1050 (a); H_2-TPR profiles of LSCrF1030 and LSCrF1050 between 550 and 900 °C (b).

Table 3
Summary of H_2 consumption (%) per gram of catalyst.

Sample	T_{max} of main peak or range of temperature (°C)	Total H_2 consumption (ml/g)
$LaCrO_3$	413	6.2
LSCrF10	355, 384, 463	23.7
LSCrF1030	348, 380, 452, ~600–850	20.8
LSCrF1050	375, 436, ~600–850	20.4

sumption compared to the undoped specimen. Such behaviour is reasonably explained by a major O^{2-} availability stemmed from the doping of A-site with lower valency element. In particular, with regard to the strontium doping effect, we observe that it markedly shapes the H_2-profile, as described by the TPR curve of LSCrF10. Since it is well established that an aliovalent ion in the A-site promotes the oxidation of a fraction of B-site cations, both Cr(IV)/Cr(III) and likely Cr(III)/Cr(II) reduction steps are related to the main peak observed between 350 °C and 600 °C. It is worth noting that both LSCrF10 and $LaCrO_3$ show in the XRD pattern traces of $SrCrO_4$ and La_2CrO_6, respectively. As a consequence, in these samples Cr(VI) should be taken into account for the reduction process [26,29]. The main reduction peak slightly shifts to lower temperature with increasing iron contents; moreover, a second broad and less intense peak appears between ~600 °C and 850 °C (Fig. 4b), which is solely associated to iron reduction, according to the literature [30–32]. Khine et al. [30] reported for Sr-doped $LaFeO_3$ a shallow reduction peak at ~400 °C, and more intense reduction signals at ~600 °C and above 900 °C, respectively. Zhang et al. observed Fe(IV)/Fe(III) reduction at $T < 300$ °C and Fe(III)/Fe(II) between 400 °C and 600 °C, even though the effective temperature ranges are influenced by the nature of dopant in B site. Thus, while the main peak of our Fe-doped samples can be related also to Fe(IV)/Fe(III) and Fe(III)/Fe(II), the second shallow peak between 600 °C and 800 °C is exclusively associated to Fe(III)/Fe(II) and Fe(III)/Fe^0 reduction steps. This last process proceeds massively over 1000 °C as it can be seen looking at the TPR curve of LSCrF1050 where the signal begins to increase at around 1000 °C [30]. From these assignments and by taking into account that only lattice oxygen is involved in the hydrogen oxidation, it is evident the striking effect of doping on reducibility of this class of materials. Even though no significant variation in H_2 consumption occurs by increasing the iron amount, the main reduction peak of LSCrF1050 shifts to lower temperatures suggesting a more favorable capacity towards reduction. Furthermore, iron extends the reduction temperature range up to 800 °C, and this is noteworthy for SOFCs working at intermediate temperature.

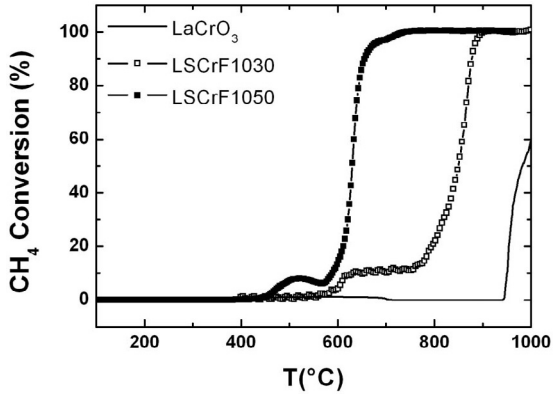

Fig. 5. Methane conversion as a function of temperature during 0.3% CH_4-TPR for $LaCrO_3$ (black line), LSCrF1030 (white squares) and LSCrF1050 (black squares).

3.4. CH_4-TPRs

3.4.1. CH_4(0.3 vol.%)/He

Preliminary TPR experiments in 0.3% CH_4 were carried out on selected samples, $LaCrO_3$, LSCrF1030, LSCrF1050 and LSCrF1550, with the intention of investigating the methane oxidation reaction when oxygen is provided exclusively by the catalyst. Fig. 5 displays the methane conversions measured by IR analyzer during CH_4-TPR (0.3 vol% in He) experiments for $LaCrO_3$, LSCrF1030 and LSCrF1050; LSCrF1550 was analyzed, but no substantial differences took place with respect to LSCrF1050, leading to the conclusion that a larger amount of Sr left unaffected the oxidation process. Actually, all samples share the same features, with the methane conversion dominated by two distinct steps, the second one being more significant with increasing the temperature. A closer analysis of the experimental data reveals that $LaCrO_3$ slightly consumes methane between ~400 °C and 700 °C and partially between ~950 °C and 1000 °C. Unlike the undoped sample, LSCrF1030 is able to consume the methane moderately between ~550 °C and 750 °C and completely from ~900 °C, whereas LSCrF1050 presents the first conversion between ~450 °C and 550 °C, and the massive conversion already at ~750 °C. The outlet gases mixture was analysed by using simultaneously IR analyzers (for CH_4, CO and CO_2 detection) and quadrupole mass spectrometer in order to detect H_2 and H_2O formation. The CO_2 and CO formation curves relative to the previously mentioned samples are shown in Fig. 6. The formation of CO_2 and water (data not shown) for all samples points to the total oxidation of methane, but, while $LaCrO_3$ and LSCrF1050 produce CO_2 essentially below 600 °C, a higher amount of carbon dioxide is formed on LSCrF1030 up to 850 °C. When the temperature

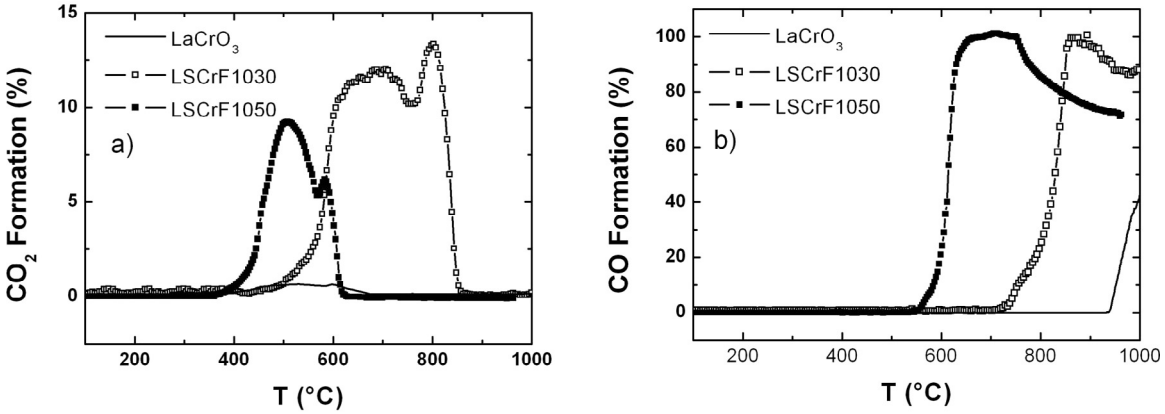

Fig. 6. CO_2 (a) and CO (b) formation curves as a function of temperature during 0.3% CH_4-TPR for $LaCrO_3$ (black line), LSCrF1030 (white squares) and LSCrF1050 (black squares).

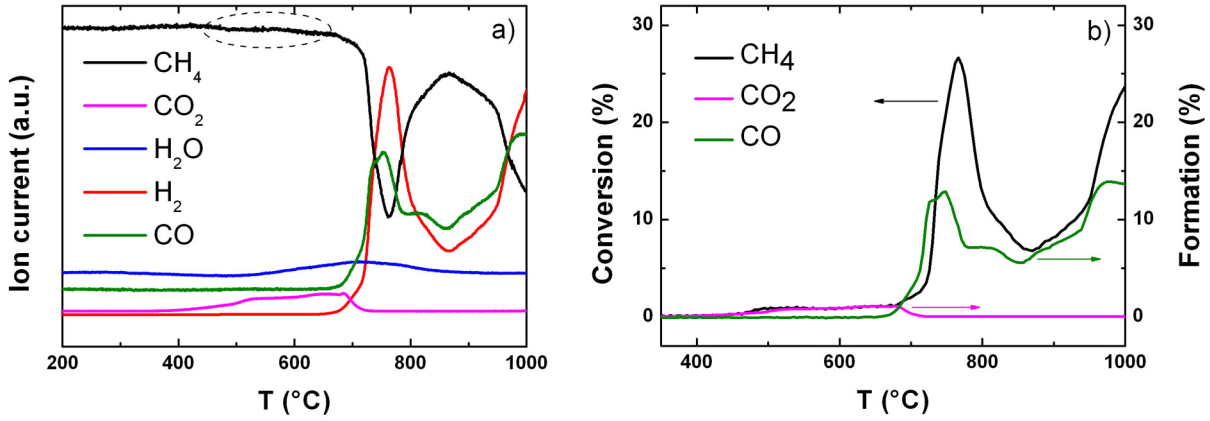

Fig. 7. MS data of LSCrF1030 during TPR in 3% CH_4 (a); CH_4 conversion and CO_2 and CO formation obtained upon LSCrF1030 during TPR in 3% CH_4 (b).

increases, CO and H_2 (data not shown) are steadily formed hinting at the partial oxidation of methane. For temperatures higher than 760 °C in the case LSCrF1050, and higher than 900 °C in the case of LSCrF1030, the CO formation decreases (Fig. 6b) even though methane continues to be consumed. This result suggests the occurrence of methane cracking reaction, which is likely competitive with the partial oxidation and preferentially occurs when all the lattice oxygen of the perovskite is consumed. Although, methane cracking is known to poison the catalyst surface because of carbon deposition [6,7], for LSCrF1030 such reaction takes place at higher temperature than for LSCrF1050 and at values out of the IT-SOFCs working range, therefore this catalyst appears more appropriate as anode material candidate.

3.4.2. CH_4 (3 vol.%)/He

In order to further evaluate the catalytic activity towards methane oxidation, TPR tests on LSCrF1030, and $LaCrO_3$ as reference, were performed in a more concentrate fuel mixture. Interestingly, by treating the sample with 3% CH_4 mixture, LSCrF1030 continues to be a catalyst for methane oxidation, as depicted in Fig. 7. In details, in the MS spectra it is easy to recognize three drops off occurring respectively at ~450 °C, ~700 °C and above ~900 °C, as well.

The shallow methane peak at lower temperature is coupled to CO_2 and water formation. This result is consistent with data previously obtained in the dilute case and demonstrates that in the same temperature range the methane is oxidized according to Eq. (1). At higher temperature, the partial oxidation takes place but, in this case, the H_2 and CO formation profiles perfectly match with the methane consumption up to 1000 °C indicating that no significant methane cracking reaction occurs. Similar methane oxidation profile was found for the undoped chromite (see Supporting information, Figs. 3.1a–3.2a) that, however, exhibits lower CH_4 conversion (see Supporting information, Table 3.1), as expected in the absence of dopants.

3.4.3. CH_4 (3 vol.%)/H_2S (150 ppm)/He

With the purpose of examining the influence of H_2S on methane oxidation, TPR experiments in 3% CH_4 and 150 ppm H_2S gas mixture were carried out on LSCrF1030 and $LaCrO_3$ as reference. In Fig. 8 MS signals and conversion profiles derived by IR analyser are shown. It is worth noting that LSCrF1030 is able to oxidize methane even if in the fuel mixture is present a potential sulphur poisoning font like H_2S. The total methane oxidation again dominates below 700 °C, while above this temperature CO and H_2 gases steadily rise, exactly corresponding to the CH_4 conversion profile. Nevertheless, methane conversion curve and CO_2, CO, H_2 profiles are somehow affected by the presence of H_2S. Indeed, in the range of temperature between 700 °C and 800 °C, much lower CH_4 conversion occurs in comparison with the reaction without H_2S, while the main process, i.e., methane partial oxidation, is registered at around 850–900 °C.

The other remarkable observation concerns the SO_2 formation between 200 °C and 550 °C, indicating that this material is a catalyst for H_2S oxidation. Quite remarkably, $LaCrO_3$ analysis leads to similar results pointing to a significant role of Cr towards both methane and H_2S oxidation (see Supporting information, Figs. 3.1b–3.2b).

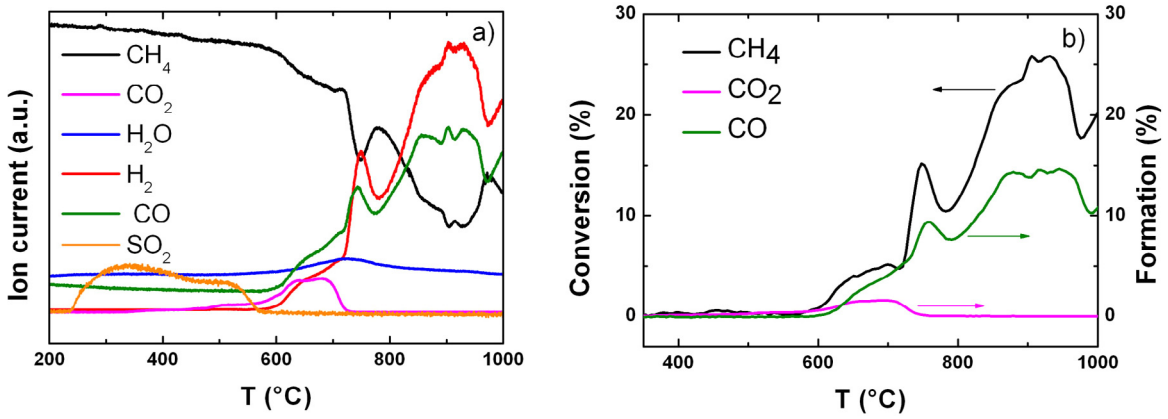

Fig. 8. MS data of LSCrF1030 during TPR in 3% CH_4 and 150 ppm H_2S (a); CH_4 conversion and CO_2 and CO formation obtained upon LSCrF1030 during TPR in 3% CH_4 and 150 ppm H_2S (b).

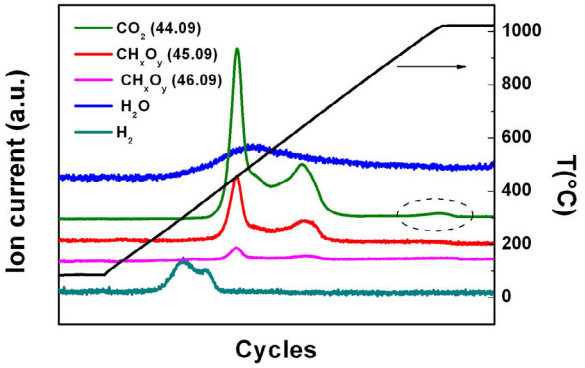

Fig. 9. MS TPO data of LSCrF1030 after TPR in 3% CH_4.

3.5. TPO

Some information about the tolerance of the catalyst towards carbon/sulphur depositions was obtained by performing TPO experiments on both LSCrF1030 and $LaCrO_3$ (see Supporting information, Fig. 4.1) after being treated in 3% CH_4 and 3% CH_4/150 ppm H_2S. Since both samples reveal comparable results, only the profiles relative to LSCrF1030 are reported in Figs. 9 and 10. A closer analysis of experimental data indicates that in both cases the reaction with O_2 induces between ~400 °C and 700 °C the formation of CO_2 and CH_xO_y species with different masses. At a first glance, these findings point to deposition on the catalyst surface during the CH_4-TPR of different carbonaceous species, like C, CH_x and CH_xO. H_2O evolution observed in the same temperature range corroborates the formation of CH_x and CH_xO species. It is worth noting that CO_2 and CH_xO_y profiles are characterized by two maxima: the former is at ~400 °C, while the latter takes place at ~500 °C and at ~600 °C after CH_4- and CH_4/H_2S-TPR, respectively. Similar results are most likely associated to a different nature of the deposits on the material. Accordingly to the considerations of Calliot et al., the lower temperature signal is due to polymorphic carbon, while the higher temperature peak is attributed to graphitic carbon [6,10,33,34].

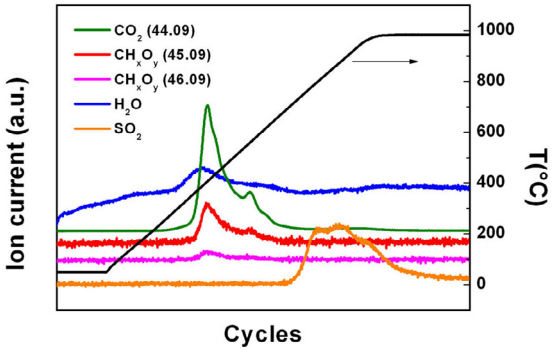

Fig. 10. MS TPO data of LSCrF1030 after TPR in 3% CH_4 and 150 ppm H_2S.

Another significant difference between the TPO experiments carried out after CH_4-TPR and CH_4/H_2S-TPR consists in the evolution of H_2 observed exclusively after the former treatment. This hydrogen could be due to storage phenomenon during the partial oxidation of methane and/or thermal decomposition of CH_x at relative low temperature.

Finally, in the case of the catalyst previously treated with CH_4/H_2S mixture, a SO_2 signal is detectable between ~600 °C and 1000 °C suggesting the presence of S_x species on the surface of this sample.

4. Discussion

The phase composition of the investigated oxides is determined by the optimal balance between Sr- and Fe- doping. Actually, only LSCrF1050 and LSCrF1550 are single-phase, whereas all the other samples doped on the A- and B- sites present a minor rhombohedral component. Tezuka et al. [18] argued that the phase composition of doped lanthanum chromites can be explained making reference to the Goldschmidt tolerance factor. According to this approach, in perovskite-type oxides lattice distortion from ideal cubic unit cell depends on the ratio between the average ionic radii of A and B ions. Considering this and taking into account that Sr(II) intake forces the charge-compensating transition of Cr(III), or Fe(III), to Cr(IV), or Fe(IV), it is clear that the phase composition depends on the relative amount of Sr, Cr and Fe and on the oxidation state of the reducible species. As reported in Table 1, the perovskite structure is retained after both CH_4 and CH_4/H_2S treatments, and no traces of metal phases were found by XRD analysis, demonstrating the stability of doped-$LaCrO_3$ under IT-SOFC temperatures and chemical environment. Nevertheless, it seems that the rhombohedral phase grows to the detriment of the orthorhombic one, likely because under reducing atmosphere the concentration of B(III) species is enhanced, favoring a less distorted structure [35]. The phase transition from orthorhombic to rhombohedral under reducing environment is probably related with the amount of oxygen release. Actually, the higher oxygen release in diluted methane (*vide infra*, Fig. 7 and related discussion) corresponds to higher rhombohedral content with respect to the sample subjected to the concentrated methane treatment (Table 1). This transition might

be considered as a drawback for the anodic performance of these materials, although it could be less important under IT-SOFC operation, due to the continuous income of O^{2-} ions from the cathode.

In most of the literature studies, H_2-TPR experiments carried out on $LaCrO_3$ do not provide consumption peaks below 900 °C since Cr(III)/Cr(II) reduction step requires higher temperatures [26,29]. Thus, our H_2-TPR results, where $LaCrO_3$ exhibits a well defined Cr reduction peak, might be related to the reduction of a small amount of Cr(VI) in agreement with the XRD results, and to the contribution of Cr(IV) present in low concentration. This hypothesis is corroborated by XPS analysis (Fig. 2) where two de-convoluted peaks are observed, one related to Cr(III/IV) and the other to Cr(VI) [22]. The same XPS signals appear for the Fe-doped samples, but, in agreement with literature, also the reduction of iron species takes place between 300 °C and 550 °C, even if the XPS spectra cannot be suitably resolved to evidence the clear presence of iron species in high oxidation state.

With respect to the methane consumption processes depicted in Fig. 5, where the doped samples are exposed to dilute methane fuel mixture, total and partial oxidations are ruled by thermodynamic control, as reported in the literature for Fe (Mn)-based $LaCrO_3$. For example, Tao and Irvine [9] carried out experiments on $La_{0.75}Sr_{0.25}Cr_{0.5}Fe_{0.5}O_{3-\delta}$ co-feeding CH_4 and O_2 at 900 °C, and found that the selectivity towards total methane oxidation is a function of molar O_2/CH_4. In particular total oxidation is promoted under O_2-rich O_2/CH_4 mixture. Indeed, van den Bossche et al. [4], performing pulse reducibility tests with CH_4/Ar gas mixture on $La_{0.75}Sr_{0.25}Cr_xMn_{1-x}O_{3-\delta}$, suggested that the selectivity towards total or partial methane oxidation depends on the oxygen stoichiometry of the catalyst. In details, the selectivity towards total methane oxidation between 700 °C and 900 °C was reduced when the O^{2-} availability decreased. Our contribution puts forward that for $La_{0.9}Sr_{0.1}Cr_yFe_{1-y}O_{3-\delta}$ between 500 °C and 850 °C the nature of oxidation processes is consistent with the existing literature. However, methane conversions of both LSCrF1030 and LSCrF1050 are quite different as concerns the range of fuel activation temperature, despite they show very similar H_2-TPR performances. Since our TPR experiments monitored the capacity to release lattice oxygen for fuel oxidation, LSCrF1050 should be considered a preferable catalyst, as long as it catalyses the total oxidation of CH_4 at lower temperature (400–600 °C) than LSCrF1030 (500–850 °C). Nevertheless, by increasing the temperature, both materials hold a reduced oxygen availability which favors the partial oxidation to CO; this process is undesirable under IT-SOFC regime, i.e., between 500 °C and 800 °C and about $pO_2 \leq 1 \times 10^{-20}$ atm. As a matter of fact, LSCrF1050 already produces CO in the IT-SOFC temperature range, while LSCrF1030 promotes the total oxidation until about 850 °C. This higher activity of LSCrF1050 toward CH_4 oxidation might rely on the different composition, and in particular on the surface composition of the first atomic layers, that are more available for interaction with the fuel. In general the CH_4-TPR studies led to the conclusion that for this class of materials the presence of iron in the B-site has a positive effect on the ability to oxidize methane. This result agrees with XPS analysis, which brings to light that effectively the surface of LSCrF1050 contains a major Fe amount compared to LSCrF1030 (Table 2). This positive influence of iron is well known in the existing literature, which in general reported that $LaFeO_3$-based oxides are more reactive compared to the $LaCrO_3$-based compounds [30]. On the other hand, no substantial differences in oxygen surface content were noticed by XPS between LSCrF1030 and LSCrF1050, confirming that reducible species play a key role in the mechanism of methane oxidation. Another important observation is related to the percentage of CO_2 and CO formation. Fig. 6 evidences that no considerable differences exist between the two studied specimens, and this behavior well fits with the reducibility tests in H_2. Thus, the amount of oxygen desorbed by the two samples is almost the same, even though the mechanism of release lattice O^{2-} depends on the nature of the fuel.

In conclusion, the most noteworthy difference between LSCrF1050 and LSCrF1030 in methane oxidation is that the former produces CO_2 and CO at lower temperatures. As LSCrF1030 manifests the preferential CO_2 formation in the IT-SOFC temperature range, we focused on this catalyst the study of reforming in richer CH_4 feedstock, also in the presence of H_2S.

The TPR performed with 3% CH_4 (Fig. 7) confirms the ability of LSCrF1030 to oxidize methane between ~450 °C and 1000 °C even when it is exposed to this highly concentrate mixture. Actually, the first important information from this type of experiment is the absence of saturation phenomena which could block the catalytic reaction with a quick formation of carbonaceous deposits on the surface. By comparing the methane conversions as a function of temperature, registered during 0.3% (Fig. 5) and 3% CH_4-TPR (Fig. 7), it results that LSCrF1030 releases more oxygen in the presence of dilute methane. Interestingly, different kinetics of O^{2-} release takes place as a function of CH_4 concentration in the gas mixture. This finding can be explained taking into account the occurrence of mass diffusion effects in the case of the TPR performed with 3% CH_4. In the experimental conditions used during the TPR (namely mass of catalyst, gas mixture flow and concentration of 3% CH_4/He), the chemical regime could not be ensured and the reaction might be affected by a diffusive regime with a consequent decrease reaction rate [36]. Then, it results that above 900 °C the perovskite still provides some lattice oxygen for methane oxidation and, as a consequence, it can be inferred that apparently no cracking reaction occurs. On the contrary, in the case of the TPR performed with 0.3% CH_4 at 900 °C, the catalyst has already consumed all lattice O^{2-} available for fuel oxidation (Figs. 5 and 6b) and methane cracking takes place predominantly.

Nonetheless, TPO performed after TPR with 0.3% and 3% CH_4 reveals evolution of CO_2 and CH_xO_y species leading to the hypothesis that different stable carbon-rich deposits (C, CH_x, CH_xO) were formed during the TPR tests. In general, it is well established that the major source of carbon deposition is the cracking of CH_4 at high temperature. The carbon deposited should be removed by O_2 producing CO_2 in a temperature range which depends on the reactivity of carbonaceous species and the strength of bond between carbon and catalyst, as well. As proposed by Gavrielatos et al. [33] in the case of Ni-based anode materials, at high T the methane dehydrogenation could be competitive with the cracking, resulting in the formation of CH_x and CH_xO deposits as schematized by the following reactions (Eqs. (4) and (5)):

$$CH_4 \rightarrow CH_x + \frac{(4-x)}{2}H_2 \quad (4)$$

$$CH_x + O_{ads} \rightarrow CH_xO \quad (5)$$

$$CH_x \rightarrow C + \frac{x}{2}H_2 \quad (6)$$

CH_x carbonaceous species might easily undergo thermal decomposition generating carbon deposition and hydrogen as indicate by Eq. (6); in an oxygen rich atmosphere both CH_x and CH_xO could be oxidized to CH_xO_2, Eq. (7). In the light of these considerations, it is worth to note that water is produced at the same time as CO_2 and CH_xO_2, and this seems to corroborate the formation of CH_xO on the catalyst surface as could be outlined by the following reaction, Eq. (8):

$$CH_xO + \frac{1}{2}O_2 \rightarrow CH_xO_2 \quad (7)$$

$$4CH_xO + (2+x)O_2 \rightarrow 4CO_2 + 2xH_2O \quad (8)$$

To the best of our knowledge, for this class of materials it has been argued neither the type of the carbonaceous deposits nor the

formation of water. For instance, Danilovic et al. [10] disclosed evidence of water production during TPO experiments for a series of differently doped perovskite-type oxides, but no hypotheses were formulated in order to correlate that finding with the type of deposit. To provide a suitable reason for the concomitant production of CO_2 and CH_xO_2, we propose that both reactions Eq. (7) and Eq. (8) take place simultaneously. In any case, independently of the poisoning nature, the deposits are removed in a temperature range suitable for IT-SOFC operation and it can be envisaged that under O^{2-} flux this capability of surface regeneration should be amplified. Beyond the proved existence of hydrogen rich species on the surface of catalyst, it is not possible to rule out that Eq. (3) takes place during TPR tests originating carbon deposits that require significant higher T for being removed by reaction with O_2. In this respect, CO_2 signal shows a shallow peak with the maximum at 1000 °C (Fig. 9) likely due to the oxidation of carbon strongly bonded to the catalyst surface.

The second main observation stemmed from TPO profiles of Fig. 9 concerns evolution of H_2 likely stored on the material surface during the TPR treatment or originated, according to Eq. (6), by cracking of CH_x species. However, since no conclusive evidence is reported in literature, it is plausible to argue that both factors are effective.

TPR measurements using H_2S-containing gas mixture (Fig. 8) confirm that LSCrF1030 is a good catalyst towards methane and, likely, towards H_2S oxidation. Nevertheless, it is necessary to outline that the ability to oxidize hydrogen sulphide is conditioned by CH_4/H_2S molar ratio [3]. Taking into account that 150 ppm H_2S is a reliable condition for CH_4-rich renewable fuels, two significant results should be emphasized: (i) the production of SO_2 between 250 °C and 600 °C; (ii) the consecutive selectivity towards total and partial methane oxidations in the presence of H_2S. Actually, H_2S is mainly oxidized to SO_2, but this process does not inhibit the total methane oxidation that starts in any case at ~450 °C, like in the absence of H_2S. This finding suggests that the presence of H_2S leaves unaltered the active sites of the catalyst, or at least has a promoting effect on methane conversion, as proposed in literature for other oxides [2,3,8].

The gas phase reaction between CH_4 and H_2S coupled up to CS_2 formation, as well as the thermal decomposition of H_2S are both endothermic reactions, and therefore, take place at high temperatures [2,3]. The main problem of carbon disulfide is that it easily decomposes forming sulphur poisoning, and in fact Danilovic et al. and Vincent et al. [3,10] reported CS_2 formation under electrochemical regime. Unfortunately, our MS instrument set-up did not permit to exclude the eventual presence of CS_2 formation.

Rising in temperature, the previously mentioned reactions become more probable; nonetheless, LSCrF1030 continues to be able to oxidize CH_4 over 800 °C. It is likely that this evidence stems from the fact that in the presence of H_2 reactions involving H_2S are displaced towards reactants [3].

Thus, LSCrF1030 and, as reported in the Supporting information (see Supporting information Fig. 4.1) $LaCrO_3$ as well, oxidizes H_2S solely according to the following reaction:

$$H_2S + 3O^{2-} \rightarrow SO_2 + H_2O + 2e^- \quad (9)$$

Nevertheless, TPO experiments carried out after TPR test (Fig. 10) and XPS data (Table 2) indicate the presence of S_x deposits on the surface of the catalysts, likely generated by the following reaction:

$$H_2S + O^{2-} \rightarrow S + H_2O + 2e^- \quad (10)$$

During TPO experiments, SO_2 evolved at high temperature hinting at a strong bond between deposited sulphur and catalyst surface. Notably, sulphur deposition does not block the methane conversion. On the contrary, the literature suggests that H_2S might have a promoting effect on methane oxidation [2,3,37,38]. Our experimental results do not support significantly this last hypothesis, as it results by comparing methane conversion, CO_2 and CO formation achieved in the presence and in the absence of hydrogen sulphide (see Supporting information, Table 3.1). In addition, the simultaneous evolution of CO_2 and CH_xO_y, observed almost in the same temperature range of 3% CH_4 experiment without H_2S, leads to the conclusion that during the TPR tests a part of active sites on the catalyst surface were blocked by carbonaceous species, and that the S poisoning does not hinder the methane reactions. As above pointed out, our data do not allow to completely elucidate the role of H_2S and to this concern further investigation is foreseen; despite this lack of information, the catalytic behaviour of LSCrF1030 in H_2S-containing fuel is promising for the formulation of IT-SOFC anodes fuelled with biogas or natural gas.

5. Conclusion

A series of $La_{1-x}Sr_xCr_{1-y}Fe_yO_{3-\delta}$ perovskite-type oxides were synthesized *via* solution combustion synthesis and studied as potential anode materials for IT-SOFC fuelled with methane-based fuels. These oxide catalysts are able to release lattice oxygen in different CH_4-based gas mixtures promoting both, total methane oxidation at lower temperature and partial methane oxidation at higher temperature, even though the reaction temperatures are function of the methane concentration.

The conversion of CH_4 is found to be higher in dilute gas mixture as compared to that registered in more concentrate conditions, pointing to a different kinetics of O^{2-} release. The formation of carbonaceous deposits upon the catalyst surface is unavoidable. The evaluation of nature of deposits formed upon LSCrF1030 revealed the presence of C- and H-rich species which are removed between 400 °C and 700 °C by supplying oxygen. Thus under IT-SOFC regime easily the catalyst may be regenerated by the continuous flux of oxygen ions.

The presence of H_2S in the fuel mixture leaves unaltered the methane oxidation reaction on LSCrF1030. This catalyst resulted also able to oxidize hydrogen sulphide to SO_2. S-rich species are deposited on the surface of the catalyst anode, but they are released starting from 600 °C. The study of the ability to direct oxide methane in H_2S-containing gas mixture makes LSCrF1030 a potential anode catalyst for IT-SOFC fed with renewable fuels.

Acknowledgments

The authors thank Francesco Giordano (ISMN-CNR, Palermo) for the XRD measurements and G. Ruggeri (ISMN-CNR, Palermo) for his support during TPR experiments. Furthermore, we acknowledge the financial support of MIUR project PRIN2010 “Celle a combustibile ad ossidi solidi operanti a temperatura intermedia alimentate con biocombustibili (BIOITSOFC)”, and PON “TESEO: Tecnologie ad alta efficienza per la sostenibilita energetica ed ambientale on-board”.

Appendix A. Supplementary data

Supplementary data associated with this article can be found, in the online version, at http://dx.doi.org/10.1016/j.apcatb.2015.06.012

References

[1] D.J.L. Brett, A. Atkinson, N.P. Brandon, S.J. Skinner, Chem. Soc. Rev. 37 (2008) 1568–1578.
[2] S.H. Cui, J.H. Li, A. Jayakumar, J.L. Luo, K.T. Chuang, J.M. Hill, L.J. Qiao, J. Power Sources 250 (2014) 134–142.
[3] A.L. Vincent, J.L. Luo, K.T. Chuang, A.R. Sanger, Appl. Catal. B 106 (2011) 114–122.

[4] M. van den Bossche, S. McIntosh, J. Catal. 255 (2008) 313–323.
[5] M. Andersson, H. Paradis, J. Yuan, B. Sundén, Int. J. Energy Res. 35 (2011) 1340–1350.
[6] T. Caillot, G. Gauthier, P. Delicheŕe, C. Cayron, F.J. Cadete Santos Aires, J. Catal. 290 (2012) 158–164.
[7] H. He, J.M. Hill, Appl. Catal. A Gen. 317 (2007) 284–292.
[8] Z. Cheng, S. Zha, L. Aguilar, D. Wang, J. Winnick, M. Liu, Electrochem. Solid-State Lett. 9 (2006) A31–A33.
[9] S. Tao, J.T.S. Irvine, Chem. Mater. 16 (2004) 4116–4121.
[10] N. Danilovic, A. Vincent, J.L. Luo, K.T. Chuang, R. Hui, A.R. Sanger, Chem. Mater. 22 (2010) 957–965.
[11] Y. Bu, Q. Zhong, D. Xu, W. Tan, J. Alloys Compd. 578 (2013) 60–66.
[12] D.E. Fowler, J.M. Haag, C. Boland, D.M. Bierschenk, S.A. Barnett, K.R. Poeppelmeier, Chem. Mater. 26 (2014) 3113–3120.
[13] S.R. Jain, K.C. Adiga, V.R. Pai Verneker, Combust. Flame 40 (1981) 71–79.
[14] A.C. Larson, R.B. Von Dreele, GSAS, General Structure Analysis System, LANSCE, MS-H805, Los Alamos National Laboratory, Los Alamos, NM 87545, USA, 1998.
[15] X. Dong, S. Ma, K. Huang, F. Chen, Int. J. Hydrogen Energy 37 (2012) 10866–10873.
[16] D.A. Shirley, Phys Rev. B: Condens. Matter Mater. Phys. 5 (1972) 4709.
[17] P.M.A. Sherwood, Practical Surface Analysis, in: D. Briggs, M.P. Seah (Eds.), Wiley, New York, 1990.
[18] K. Tezuka, Y. Hinatsu, A. Nakamura, T. Inami, Y. Shimojo, Y.J. Morii, J. Solid State Chem. 141 (1998) 404–410.
[19] K.R. Chakraborty, S.M. Yusuf, P.S.R. Krishna, M. Ramanadham, A.K. Tyagi, V. Pomjakushin, J. Phys.: Condens. Matter 18 (2006) 8661–8672.
[20] K. Oikawa, T. Kamiyama, T. Hashimoto, Y. Shimojyo, Y. Morii, J. Solid State Chem. 154 (2000) 524–529.
[21] R.D. Shannon, C.T. Prewitt, Acta Crystallogr. B 25 (1969) 925–946.
[22] K. Rida, A. Benabbas, F. Bouremmad, M.A. Peña, A. Martìnez-Arias, Catal. Commun. 7 (2006) 963–968.
[23] B. Liu, L. Tang, Y. Zhang, Int. J. Hydrogen Energy 34 (2009) 440–445.
[24] D. Hari Prasad, S.Y. Park, E.O. Oh, H. Ji, H.R. Kim, K.J. Yoon, J.W. Son, J.H. Lee, Appl. Catal. A 447–448 (2012) 100–106.
[25] P.A.W. van der Heide, Surf. Interface Anal. 33 (2002) 414–425.
[26] V.B. Vert, F.V. Melo, L. Navarrete, J.M. Serra, Appl. Catal. B 115–116 (2012) 346–356.
[27] P. Kumar, R. Kumar Singh, A.S.K. Sinha, P. Singh, J. Alloys Compd. 576 (2013) 154–160.
[28] D. Xu, Y. Bu, W. Tan, Q. Zhong, Appl. Surf. Sci. 268 (2013) 246–251.
[29] A. Kaddouri, S. Ifrah, G. Bergeret, Catal. Lett. 129 (2009) 336–343.
[30] M.S.S. Khine, L. Chen, S. Zhang, J. Lin, S.P. Jiang, Int. J. Hydrogen Energy 38 (2013) 13300–13308.
[31] R. Zhang, A. Villanueva, H. Alamdari, S. Kaliaguinea, J. Catal. 237 (2006) 368–380.
[32] P. Ciambelli, S. Cimino, L. Lisi, M. Faticanti, G. Minelli, I. Pettiti, P. Porta, Appl. Catal. B 33 (2001) 193–203.
[33] I. Gavrielatos, V. Drakopoulos, S.G. Neophytides, J. Catal. 259 (2008) 75–84.
[34] N.C. Triantafyllopoulos, S.G. Neophytides, J. Catal. 239 (2006) 187–199.
[35] A.M. Glazer, Acta Cryst. B 28 (1972) 3384–3392.
[36] S.K. Bhatia, D.D. Perlmutter, AIChE J. 27 (1981) 247–254.
[37] G. Postole, F. Bosselet, G. Bergeret, S. Prakash, P. Gélin, J. Catal. 316 (2014) 149–163.
[38] A. Kaddouri, B. Béguin, Catal. Commun. 46 (2014) 22–27.